ResearchGate

See discussions, stats, and author profiles for this publication at: https://www.researchgate.net/publication/229577272

Surface-enhanced Raman spectroscopic analysis of fonofos pesticide adsorbed on silver and gold nanoparticles

ARTICLE *in* JOURNAL OF RAMAN SPECTROSCOPY · OCTOBER 2010

Impact Factor: 2.67 · DOI: 10.1002/jrs.2579

CITATIONS
33

READS
103

3 AUTHORS, INCLUDING:

Jitraporn Vongsvivut
Australian Synchrotron
33 PUBLICATIONS **178** CITATIONS
SEE PROFILE

Evan G Robertson
La Trobe University
95 PUBLICATIONS **1,782** CITATIONS
SEE PROFILE

Available from: Jitraporn Vongsvivut
Retrieved on: 27 January 2016

Research Article

Journal of RAMAN SPECTROSCOPY

Received: 5 August 2009 Accepted: 2 November 2009 Published online in Wiley Online Library: 26 January 2010

(wileyonlinelibrary.com) DOI 10.1002/jrs.2579

Surface-enhanced Raman spectroscopic analysis of fonofos pesticide adsorbed on silver and gold nanoparticles

Jitraporn Vongsvivut,[a] Evan G. Robertson[a,b] and Don McNaughton[a]*

Surface-enhanced Raman scattering (SERS) spectra of fonofos, an organophosphorous pesticide (OPP), were recorded using citrate-reduced silver (Ag) and gold (Au) colloidal nanoparticles in the form of dried films. In this study, significant enhancements were achieved with fonofos concentrations down to ~10 ppm with the Ag colloids, demonstrating a potential for the technique in the analysis of fonofos residues. Successful formation of the SERS-active metal aggregates was indicated by the presence of a plasmon band at longer wavelengths in the UV–visible spectrum. Transmission electron microscopy (TEM) images revealed distinctively different morphologies of the aggregates formed by the two metals, while the observed SERS spectral features of fonofos were also found to be different for molecules adsorbed on Ag and Au colloidal surfaces. This evidence suggests metal-induced changes in adsorption behavior of the fonofos analyte, leading to the different binding structures onto the different metal surfaces. Comparisons between the most prominent SERS-enhanced bands and the precise mode descriptions predicted through density functional theory (DFT) simulations at the B3LYP/6-311+G(d,p) level allowed an in-depth orientation analysis of the adsorbed species on metal surfaces. Nevertheless, the ring vibrations were found to possess a major contribution in the observed SERS enhancements for both metal nanoparticles. **Copyright © 2010 John Wiley & Sons, Ltd.**

Supporting information may be found in the online version of this article.

Keywords: SERS; organophosphorus pesticide; fonofos; density functional theory; B3LYP/6-311+G(d,p)

Introduction

Organophosphorus pesticides (OPPs) have become one of the most commonly used groups of pest control chemicals in agriculture throughout the world. The toxicity induced by organophosphates results from inhibiting the enzymes acetylcholinesterases (ChE) in the nervous system of the exposed organisms in either target pests or humans. These enzymes remove acetylcholine (Ach), which carries electrical signals across the synapse, leading to rapid twitching of voluntary muscles and finally paralysis or heart failure.[1] Despite acute poisoning caused by an exposure to OPPs, the use of OPPs has been progressively increasing over the past years, and this has attracted intense public concern worldwide about trace amounts of the residues in agricultural products that might cause long-term non-fatal health effects. A continual improvement in analytical techniques has therefore played a vital role in monitoring chemical residues in foods in order to assure safety for the consumers and to achieve optimal regulation for pesticide uses.

According to a review by the US Geological Survey National Water Quality Laboratory (USGS),[2,3] the standard routine analysis for trace pesticide residue is based mainly on gas chromatography (GC) with flame photometric detection offering an excellent limit of detection (LOD) down to sub-parts-per-million. The advantage of using GC arises from its high separation power and, in addition, sensitivity and/or selectivity can be achieved through a selection of detectors such as electron capture detector (ECD),[4] nitrogen–phosphorus detector (NPD),[5] and mass spectrometry (MS).[6,7] Liquid chromatography coupled to MS (LC–MS) has also been demonstrated in recent years to be a potential technique particularly for determination of pesticides of low volatility and thermolability.[8,9] However, sample preparations and extraction process in the chromatographic techniques are time consuming, and require extensive manual handling of toxic pesticide samples as well as large amounts of organic solvents. The sophisticated combinations of instrumentation required for the measurements are also disadvantages of the techniques.

We accordingly introduce a highly sensitive surface-enhanced Raman scattering (SERS) spectroscopic technique as an alternative in pesticide analysis. Since its first discovery,[10] the SERS technique has been rapidly developed as a potential trace method widely used in numerous applications for detecting molecules and/or monolayers on a variety of rough metal surfaces,[11] providing an enhancement in the Raman scattering signal by up to 10^6 or even 10^{10}. Indeed the exquisite sensitivity of the technique, which has been proved to be sufficient for single-molecule detection,[12,13] is the result of the electromagnetic (EM) field, which is greatly amplified through the excitation of localized plasmon resonance inside the metal nanoparticles.[14] As a consequence, the signal of molecules in a close proximity to the surface of the metal is intensified due to the coupling of the enhanced EM field to the molecular vibrations, leading to a large increase in the

* *Correspondence to: Don McNaughton, Centre for Biospectroscopy, School of Chemistry, Monash University, Wellington Road, Clayton, Victoria 3800, Australia. E-mail: Don.McNaughton@sci.monash.edu.au*

a *Centre for Biospectroscopy, School of Chemistry, Monash University, Clayton, Victoria 3800, Australia*

b *Department of Chemistry, La Trobe University, Bundoora, Victoria 3086, Australia*

Copyright © 2010 John Wiley & Sons, Ltd.

Raman cross section, and when combined with an optical Raman microscopic approach can be achieved at micron spatial resolution. In addition, the basic advantage of using Raman spectroscopy is that the technique allows samples to be measured inside a closed glass container to prevent possible toxicity making it suitable for examining toxic chemicals.

In this paper we demonstrate the application of the micro-SERS technique for trace detection of an OPP analyte in parts per million concentration levels using citrate-reduced metal colloidal nanoparticles. Fonofos was selected as the model OPP because of the public concern regarding fonofos pesticide residues in US agricultural products.[15] The observed spectra were analyzed by comparison with the normal Raman spectra of fonofos after a detailed assignment of the vibrational modes provided by density functional theory (DFT) calculations at the B3LYP/6-311+G(d,p) level. This analysis provides information on the molecular orientation of the model pesticide adsorbed on surfaces of Ag and Au nanoparticles.

Experimental

Materials and reagents

Fonofos (Dyfonate®, *O*-ethyl *S*-phenyl ethylphosphonodithioate) was used as purchased in analytical standard grade (≥99% purity; Sigma-Aldrich, New South Wales, Australia) without further purification. All glassware was rigorously cleaned before use by treatment with aqua regia (HNO_3 + HCl = 1 : 3 v/v) followed by thorough rinsing with plentiful distilled water and purging with nitrogen gas. Due to its hydrophobicity and the limited solubility of the analyte in water, a stock solution of 10% fonofos was prepared by a subsequent dilution in high purity methanol as recommended for residue analysis (PESTANAL®, ≥99.9%). Aliquots of the stock solution were made up into a range of concentrations down to 0.01% (equivalent to ~110 ppm).

Citrate-reduced silver (Ag) and gold (Au) colloidal solutions were prepared by a method based on Lee and Meisel's standard procedure[16] because of the reported superior stability over borohydride-reduction methods.[17] The preparation of the Ag nanoparticles started by dissolving 90 mg of $AgNO_3$ in 500 ml of 18 MΩ ultrapure water, and bringing the aqueous solution to boil with extensive stirring. Ten milliliters of 1% sodium citrate was then added dropwise and the solution kept at boiling for ~90 min. This procedure produced a turbid gray Ag colloidal solution with λ_{max} = 410 nm, which corresponds to the excitation of a dipolar surface plasmon of Ag spheres having radii of ~10–30 nm in water.[18]

A similar procedure was applied for the preparation of the Au nanoparticles, except for the quantity of chemicals used in the reaction. Briefly, 240 mg of $HAuCl_4$ was dissolved in 500 ml of 18 MΩ ultrapure water, and the aqueous solution was brought to boil with extensive stirring. Then 50 ml of 1% sodium citrate was added dropwise and the solution was kept boiling for ~90 min. The complete citrate reduction finally resulted in a clear wine-red Au colloidal solution with an observed λ_{max} = 520 nm, which corresponds to radii of colloidal Au particles in the range of 10–30 nm.[18,19] The observed full width at half height (FWHH) for both metal colloids prepared in this work was within ~80–120 nm, indicating a moderate polydispersity of these metal colloidal solutions.[18]

To determine the effect of aggregating agents toward SERS activity, 1 ml of each metal colloidal solution was mixed with 40–80 µl of 0.05 M of various anionic solutions (i.e. NaCl, Na_2SO_4, and KNO_3). Fonofos in methanol solution (100 µl) was then added to the mixture and left for 5 min to ensure complete aggregation. As a consequence, the actual concentration of fonofos in the final mixture was decreased to 0.09 times its original concentration (i.e. ~10 ppm for 0.01% original solution). A similar preparation without the use of any aggregating agent was also performed for a comparison. Only 10 µl of the final solution, so-called SERS-active mixture, was dropped onto an aluminum-coated microscope slide and air-dried prior to Raman microscopic measurements.

Experimental parameters for spectroscopic measurements

UV–visible spectroscopy

The UV–visible absorption spectra of the metal colloidal solutions before and after the aggregation process were recorded at a resolution of 1 nm with a Cary 100 Bio UV–visible spectrophotometer using a 1-cm quartz cuvette.

SERS and Raman spectroscopy

Raman and SERS measurements were conducted using a Renishaw InVia Raman microspectrometer (Renishaw, New Mills, UK), which was equipped with a 633-nm HeNe laser (Model 05-LHP-928, Coherent Scientific, Santa Clara, CA, USA) and a thermo-electrical cooled charge-coupled device (CCD) detector. The original laser power measured at the sample of ~12 mW was reduced to 1–6 mW to prevent heating and photochemical damage. Exposure time used for data collection was typically 10 s, otherwise as stated individually. An initial spectral collection was performed repeatedly to monitor the complete evaporation of solvent (i.e. methanol) from the dried metal-cooperated fonofos films and SERS measurements were initiated when no spectroscopic evidence of solvent remained in the spectra. Each spectrum shown is an average of 10 spectra collected from various locations within the dried film under identical conditions. Spectral analysis was performed using OPUS (Bruker Optik GmbH) and GRAMS32 (Galactic Industries Corporation) software.[20]

DFT calculations

DFT calculations were performed to investigate the structural and spectroscopic features of fonofos (in the gaseous state), using Gaussian 03 software.[21] The hybrid of Becke's non-local three parameter exchange and correlation functional with the Lee–Yang–Parr correlation functional (B3LYP) was used, with a split valence-shell 6-311+G(d,p) basis set augmented by d- and p-polarization functions on heavy and hydrogen atoms. A series of geometry optimizations was performed in order to locate the global potential energy minima. Starting structures were selected from the lowest-energy conformers obtained through an initial structural optimization using a semi-empirical (AM1) method in Hyperchem software (Version 8.0.4, Hypercube Inc., Gainesville, FL, USA).

To simulate a Raman spectrum, the Raman activities (S_i) calculated with the Gaussian 03 software were subsequently converted into relative Raman intensities (I_i) using the following equation as previously described elsewhere[22,23] and Lorentzian band shapes were applied with a FWHH of 10 cm^{-1}. Simulated

Copyright © 2010 John Wiley & Sons, Ltd.

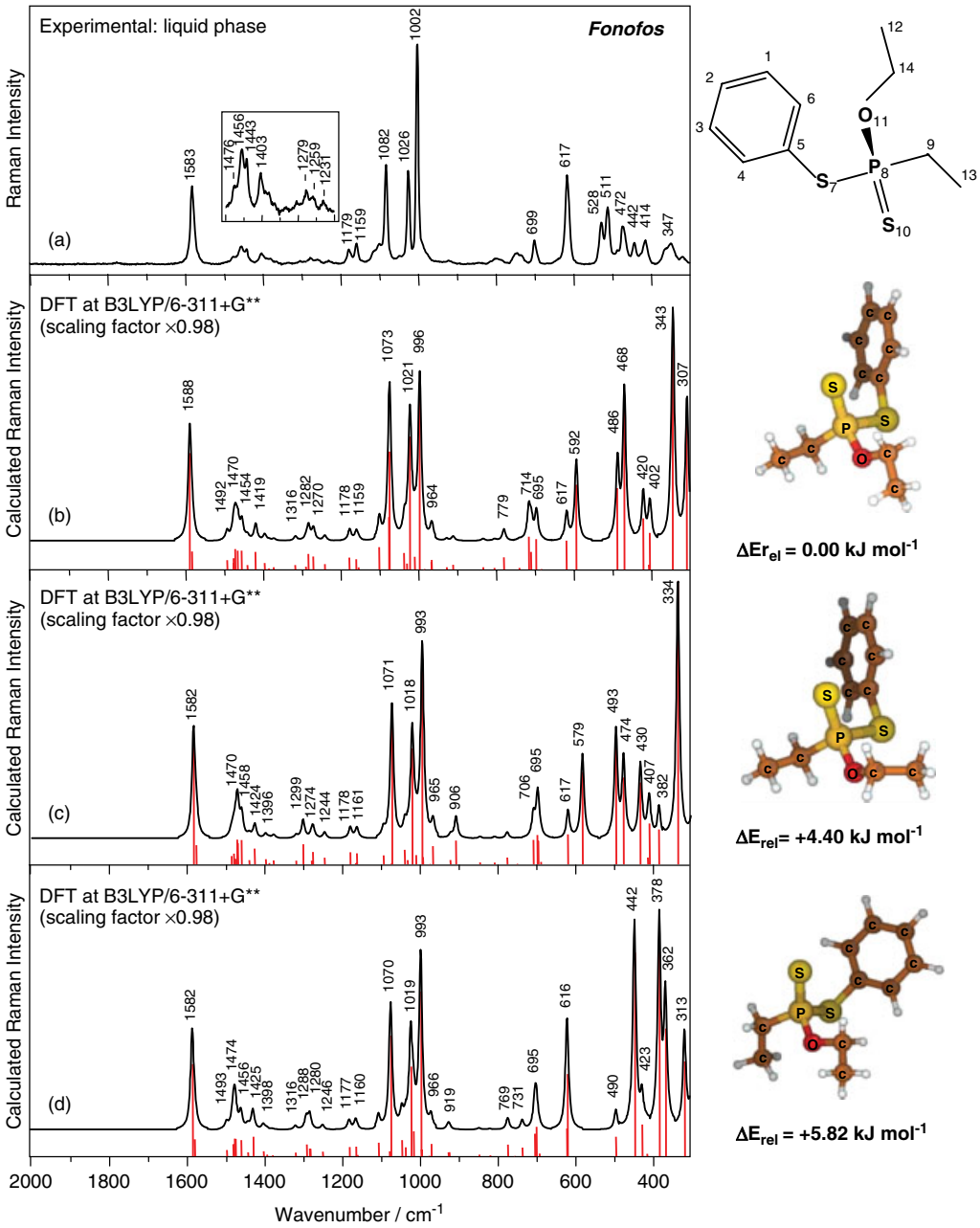

Figure 1. (a) The experimentally observed Raman spectrum of fonofos collected using 633-nm excitation wavelength (left), and molecular structure of fonofos with the atom numbering used for specifying mode descriptions in Table 1 (right). (b–d) Simulated and stick theoretical Raman spectra (left) of the corresponding three lowest-energy B3LYP/6-311+G(d,p)-optimized structures of fonofos displayed in association with zero-point corrected relative energies (right).

Raman spectra of the various conformers were then correlated with the corresponding experimental Raman spectrum.

$$I_i = \frac{f(\nu_0 - \nu_i)^4 S_i}{\nu_i \left[1 - \exp\left(-\frac{hc\nu_i}{kT}\right)\right]} \quad (1)$$

where ν_0 is the excitation wavenumber in cm^{-1} (ν_0 = 15797.79 cm^{-1} corresponding to the wavelength of 633 nm of the HeNe laser used in this study); ν_i is the vibrational wavenumber of the ith normal mode; h, c, and k are fundamental constants; T is temperature in Kelvin (K); and f is an appropriate normalization factor for all peak intensities.

Results and Discussion

Comparisons of DFT calculations and the experimental Raman spectra

Our preliminary calculations clearly showed that the accuracy of predicted vibrational wavenumber values and relative intensities was significantly improved by adding diffuse functions (+) to all the atoms and increasing the level of the basis set (i.e. from 6-31G(d,p) to 6-311+G(d,p)) as shown in Fig. S1 (Supporting Information). Therefore, in spite of the additional computational time required, the 6-311+G(d,p) basis set was selected for the study. Figure 1(a) presents the experimental Raman spectrum of

Copyright © 2010 John Wiley & Sons, Ltd.

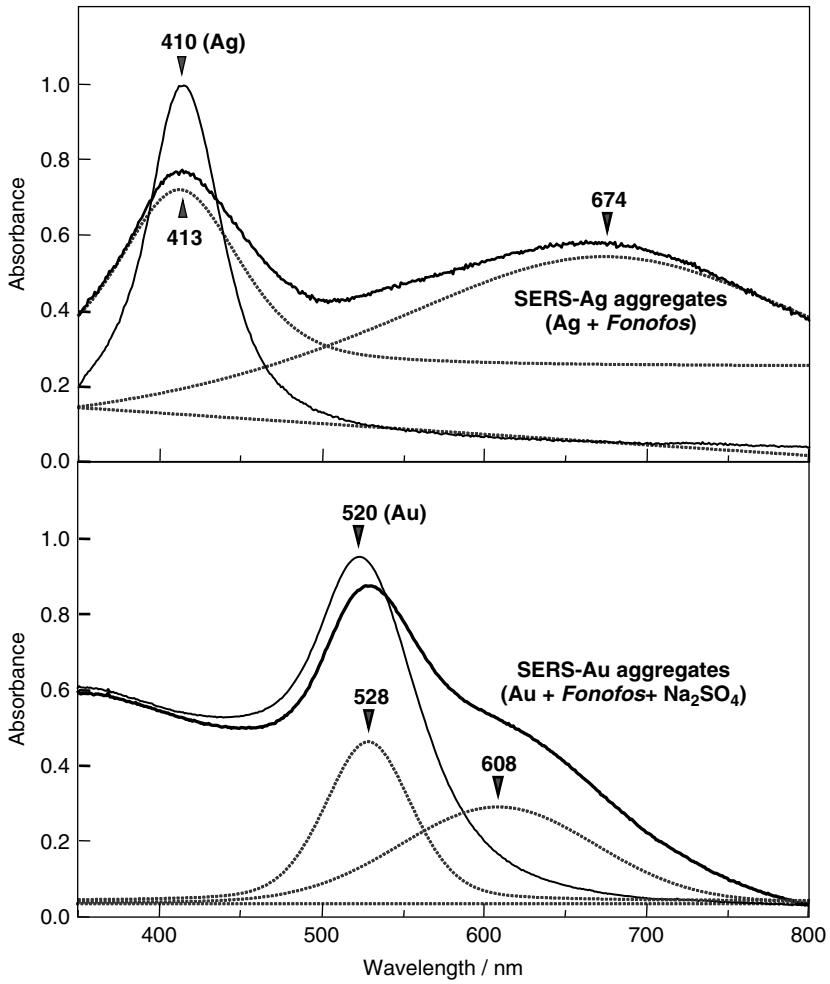

Figure 2. UV–visible spectra of the citrate-reduced metal nanoparticles (–) and their SERS-active aggregates with fonofos (—). Dashed lines (· · · ·) represent fitting results of the SERS aggregate spectra in order to clearly present the feature and the position of the plasmon band produced in the visible region after a successful formation of SERS-active fonofos–metal aggregates.

fonofos in comparison to the simulated Raman spectra of the three lowest-energy conformers (Fig. 1(b)–(d)) obtained from the DFT calculations. In all cases, the calculated vibrational wavenumber values were scaled using the general anharmonic scaling factor of 0.98 for this basis set in order to reduce the deviation between experimental and theoretical values. As seen in Fig. 1, the major difference in the optimized structures is the orientation of the two ethyl groups which leads to a significant variation in the simulated spectral profiles in the low-wavenumber region ($\leq$850 cm^{-1}), while the fundamental vibrational modes obtained in the higher-wavenumber region appear to be very similar for all structures and correlate well with those observed in the normal Raman spectrum.

In the high-wavenumber spectral range ($\geq$850 cm^{-1}), the spectrum is dominated by an intense band at 1583 cm^{-1} attributable to ν(C═C) vibration of the phenyl ring, and a triad of bands at 1082, 1026, and 1002 cm^{-1}, which are assigned to the ν(S–C_{phenyl}) stretching vibration in association with in-plane δ(C_{phenyl}–H) deformations of the phenyl ring, and two benzene-like modes of δ(CCC) vibrations, respectively. It should be noted that our band assignments for the triad, which are based on the DFT calculations of fonofos reported herein for the first time, contradict those previously published for SERS of fonofos in which the bands were attributed to symmetric stretches of the central P atom (i.e. SPO and POC).[24,25] Our band assignment is however consistent with the observation of a similar triad in the Raman spectrum of thiophenol.[26] The absence of P/O atoms in thiophenol confirms that these bands are benzene-ring related vibrations. This accordingly demonstrates the value of the DFT results in providing a reliable interpretation for vibrational modes.

Considering the spectral profile within the range of 550–850 cm^{-1}, it is found that the predicted Raman spectrum of the conformer *d* provides the best match to that of the experimental spectrum, particularly for the strong peak centered at 616 cm^{-1}. This band, which is substantially downshifted to 592 and 579 cm^{-1} in case of the conformers *b* and *c*, represents combined stretching modes of the central atoms including ν(P–S), ν(P═S), and ν(P–C) vibrations, respectively. Contrary to this, conformer *c* provides a better match for the modes present in the low-wavenumber region ($\leq$550 cm^{-1}). Bands in this region arise mainly from out-of-plane ring deformations as well as stretching and deformation vibrations of the central atoms. Despite the dissimilarity of spectral profile in the range of 550–850 cm^{-1}, conformer *c* is shown to provide the best correlation with the experimental spectrum in most of the spectral range, and is thereby chosen as the main reference structure for the mode assignments, even though the conformer did not possess the global energy

Copyright © 2010 John Wiley & Sons, Ltd.

Table 1. Raman wavenumber values (cm^{-1}) and mode descriptions of fonofos (conformer *c*) obtained from the theoretical DFT calculations at B3LYP/6-311+G(d,p) level and the experimental normal Raman spectroscopy (NRS)/SERS measurements

	Theoretical B3LYP/6-311+G(d,p)		Experimental				
Mode	Position[a] (cm^{-1})	Intensity[b] Å^4/AMU	NRS (cm^{-1})	SERS Ag (cm^{-1})	SERS Au (cm^{-1})	Plane	Mode descriptions[c]
81	3123	3.6	3150	3150	3150	In	ν(C6–H) + ν(C–H)$_{phenyl}$ (mode 2)
80	3108	9.1	–	–	–	In	ν(C–H)$_{phenyl}$ (mode 20a)
79	3101	4.2	–	–	–	In	ν(C–H)$_{phenyl}$ (mode 20b)
78	3090	5.2	3063	3062	3062	In	ν(C–H)$_{phenyl}$ (mode 7b)
77	3081	2.0	–	–	–	In	ν(C–H)$_{phenyl}$ (mode 13)
76	3037	0.42	–	–	–	In	ν_{asym}(C12–H) + ν_{asym}(C14–H)
75	3036	0.66	–	–	–	In	ν_{asym}(C13–H) + ν_{asym}(C9–H)
74	3018	3.8	–	–	–	In	ν(C13–H) (t_2 symmetry) + ν(C9–H)
73	3017	3.7	–	–	–	In	ν(C12–H) (t_2 symmetry) + ν(C14–H)
72	3011	4.8	3022	–	–	In	ν_{asym}(C14–H) + ν(C12–H) (t_2 symmetry)
71	3010	3.6	–	–	–	In	ν_{asym}(C9–H) + ν(C13–H) (t_2 symmetry)
70	2973	5.8	2981	2979	2979	In	ν_{sym}(C14–H)
69	2967	4.3	2939	2938	2938	In	ν_{sym}(C9–H)
68	2956	9.7	2917	2914	2914	In	ν(C13–H) (a_1 symmetry)
67	2953	9.6	2881	2880	2880	In	ν(C12–H) (a_1 symmetry)
66	1582	7.9	1583	1582	1582	In	ν(C=C)$_{phenyl}$* (mode 8a)
65	1575	1.3	–	–	1576[d]	In	ν(C=C)$_{phenyl}$ (mode 8b)
64	1484	0.54	–	–	–	In	$\delta_{scissor}$(C14–H) + δ(C12–H) (*e* symmetry)
63	1477	0.72	1476	1474	1473	In	δ(C13–H) (*e* symmetry)
62	1474	0.37	–	–	–	In	ν(C=C)$_{phenyl}$+* (mode 19a)
61	1470	1.7	1456	1453	1455	In	δ(C12–H) (*e* symmetry) + $\delta_{scissor}$(C14–H)
60	1468	1.4	–	–	–	In	δ(C13–H) (*e* symmetry)
59	1458	1.6	1443	1441	1441	In	δ(C12–H) (*e* symmetry)
58	1438	0.26	–	–	–	In	ν(C=C)$_{phenyl}$+* (mode 19b)
57	1424	1.1	1403	1400	1402	In	$\delta_{scissor}$(C9–H)
56	1396	0.34	–	–	–	Out	δ(C12–H) (umbrella) + γ_{wag}(C14–H)
55	1387	0.08	–	–	–	Out	δ(C13–H) (umbrella)
54	1375	0.26	–	–	–	Out	γ_{wag}(C14–H) + δ(C12–H) (umbrella)
53	1317	0.23				In	δ(C–H)$_{phenyl}$ (mode 3)
52	1299	1.3	1279	–	–	Out	γ_{twist}(C14–H) + δ(C12–H) (t_2 symmetry)
51	1278	0.23	–	–	–	In/out	ν(C=C)$_{phenyl}$ (mode 14) + γ_{wag}(C9–H)
50	1274	0.83	1259	–	–	Out	γ_{wag}(C9–H) + δ(C13–H) (t_2 symmetry)
49	1244	0.44	1231	–	–	Out	γ_{twist}(C9–H) + δ(C13–H) (t_2 symmetry)
48	1178	0.82	1179	1181	1177	In	δ(C–H)$_{phenyl}$ (mode 9a)
47	1164	0.07				In/out	δ_{rock}(C14–H) + δ(C12–H) (t_2 symmetry) + τ(O–C14–C12–H)
46	1161	0.74	1159	1157	1158	In	δ(C–H)$_{phenyl}$ (mode 15)
45	1093	0.60	–	–	–	In	δ(C12–H) (t_2 symmetry) + $\delta_{scissor}$(O–C14–C12)
44	1074	0.03	–	–	–	In	δ(C–H)$_{phenyl}$ (mode 18b)
43	1071	10	1082	1079	1081	In	ν(S–C$_{phenyl}$) + δ(C–H)$_{phenyl}$ (mode 18a)
42	1037	0.98	–	–	–	In/out	γ(C9–H) + δ(C13–H) (t_2 symmetry) + ν(C9–C13) + ν_{asym}(O–C14–C12)
41	1030	0.28	–	–	–	In/out	γ(C9–H) + δ(C13–H) (t_2 symmetry) + ν_{asym}(O–C14–C12) + ν(C9–C13)
40	1018	7.8	1026	1023	1024	In	δ(C–H)$_{phenyl}$ (mode 18a) + ν(S–C$_{phenyl}$)
39	1008	0.62	–	–	–	In/out	τ(C9–C13) + ν_{asym}(O–C14–C12) + γ_{twist}(C9–H) + δ(C13–H) (t_2 symmetry)
38	993	14	1002	1000	1001	In	δ(CCC)$_{phenyl}$ (mode 12)
37	990	0.47	–	–	–	Out	γ(C–H)$_{phenyl}$ (mode 5)
36	974	0.01	–	–	–	Out	γ(C–H)$_{phenyl}$ (mode 17a)

Copyright © 2010 John Wiley & Sons, Ltd.

Table 1. (*Continued*)

Mode	Theoretical (B3LYP/6-311+G**) Position[a] (cm^{-1})	Theoretical (B3LYP/6-311+G**) Intensity[b] Å^4/AMU	Experimental NRS (cm^{-1})	Experimental SERS Ag (cm^{-1})	Experimental SERS Au (cm^{-1})	Plane	Mode descriptions[c]
35	965	1.2	–	–	–	In	ν(C9–C13)
34	919	0.29	–	–	–	Out	γ(C–H)$_{phenyl}$ (mode 17b)
33	906	1.6	–	–	–	In	ν_{sym}(O–C14–C12) + δ(C14–C12–H) + ν_{asym}(P–O–C14)
32	844	0.13	–	–	–	Out	γ(C–H)$_{phenyl}$ (mode 10a)
31	806	0.11	–	–	–	In/out	τ(P–O–C14–H) + τ(C12–C14) + τ(C12–C14) + γ_{rock}(C14–H) + γ_{rock}(C12–H)
30	773	0.46	–	–	–	Out	τ(S–P–C9–H) + τ(C9–C13) + τ(O–P–C9–H) + τ(S=P–C9–H)
29	748	0.04	–	–	–	Out	γ(C–H)$_{phenyl}$ (mode 11)
28	706	1.6	–	–	–	In/out	ν(P–C9) + ν(P=S) + τ(C9–C13) + τ(O–P–C9–H)
27	695	2.0	699	696	698	In/out	ν(S–C$_{phenyl}$) + δ(CCC)$_{phenyl}$ (mode 6a) + ν(P–O) + τ(C9–C13)
26	694	1.6	–	–	–	In/out	τ(C9–C13) + ν(P–O) + τ(S=P–C9–H) + τ(O–P–C9–H) + ν(P–C9) + τ(C12–C14)
25	686	0.16	–	–	–	Out	γ(CCC)$_{phenyl}$ (mode 4)
24	617	2.0	617	614	614	Out	γ(CCC)$_{phenyl}$ (mode 6b)
23[e]	579	6.2	–	–	–	In	ν(P–S) + ν(P=S) + ν(P–C9)
22	493	7.9	528	526	526	In/out	γ(CCC)$_{phenyl}$* (mode 16b) + ν(P–S) + τ(S=P–O–C14) + $\delta_{scissor}$(P–S–C$_{phenyl}$)
21	474	5.9	511	510	510	In/out	γ(CCC)$_{phenyl}$* (mode 16b) + τ(S=P–O–C14) + ν(P–S) + τ(P–O–C14–C12) + $\delta_{scissor}$(P–C9–C13)
20	430	5.5	472	471	470	In/out	τ(C12–C14) + $\delta_{scissor}$(P–O–C14) + $\delta_{scissor}$(O–C14–C12)
19	411	0.45	–	–	–	Out	γ(CCC)$_{phenyl}$* (mode 16a)
18	407	2.7	442	441	441	In/out	ν(S–C$_{phenyl}$) + γ(CCC)$_{phenyl}$* (mode 16a) + τ(C12–C14)
17	382	2.3	414	419	415	In/out	$\delta_{scissor}$(P–O–C14) + τ(C12–C14) + τ(S(=)–P–O–C14) + τ(P–O–C14–C12) + τ(C9–P–O–C14)
16	334	19	347	345	345	In/out	ν(P–S) + $\delta_{scissor}$(P–C9–C13) + γ(CCC)$_{phenyl}$* (mode 16b)

[a] Scaling factor of 0.98.
[b] Relative Raman intensities calculated by Eqn (1) and normalized to 100.
[c] See Ref. [27] for detailed description of benzene-ring modes (ν: stretch, δ: in-plane deformation, γ: out-of-plane deformation, τ: torsion); (*) the motion appears as (CCC+CH) and (+) degenerated vibration; mode descriptions at certain wavenumber values were written in an order of relative weight (%) from higher to lower percentage.
[d] Band splitting present only in SERS of the Au–fonofos aggregates.
[e] In case of the experimental and predicted Raman spectra (conformer *d*), this mode shifted upward to higher wavenumber values resulting in an almost superposition of modes 23 and 24 as evidenced by the prominent single band observed at 617 cm^{-1} in Fig. 1(a) and (d), respectively.

minimum. In fact, the slight difference in the relative energy (i.e. $\Delta E_{rel} \leq 6$ kJ mol^{-1}) suggests that all the three conformers are likely to be present in the liquid phase and solvent effect may alter their relative stabilities by a few kilojoules per mole. Therefore, we also combined the mode descriptions obtained from conformer *d*, in addition to those of conformer *c*, for the modes present in the range of 550–850 cm^{-1}. These two conformers will be further used as reference structures for orientation analysis, despite the fact that neither structure is the global minimum for the gas phase. Given in Table 1 is accordingly a detailed correlative assignment of the calculated normal modes to the vibrational bands observed in the normal Raman spectrum of fonofos in liquid phase, with the descriptions of the normal modes using the nomenclature of benzene-like vibrations.[27]

Formation of SERS-active aggregates investigated by UV–visible spectroscopy and transmission electron microscopy (TEM)

Since the adsorption of analyte molecules on the metal colloidal particles is a primary prerequisite to achieve an effective SERS response, aggregation of the colloidal system and optimization of the nanoparticle surface charge is crucial for activation. For some

Copyright © 2010 John Wiley & Sons, Ltd.

Journal of RAMAN SPECTROSCOPY

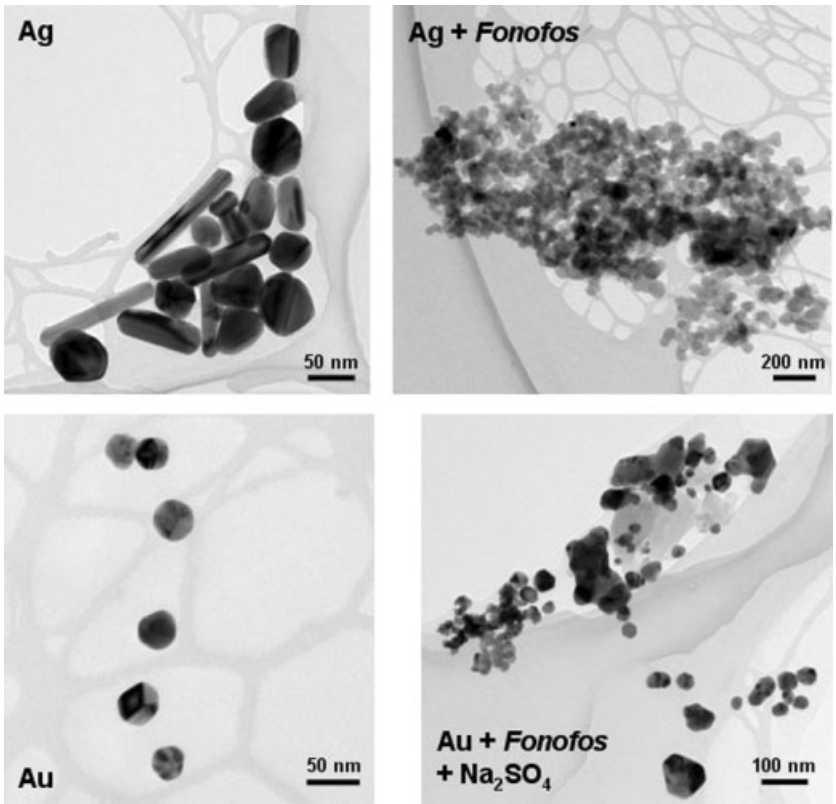

Figure 3. TEM images of the prepared citrate-reduced metal nanoparticles before and after the formation of the metal aggregates with fonofos.

analytes, an aggregation of the colloid can be induced simply by adding an aliquot of the analyte solution into the metal colloidal solution. However, where the analyte itself cannot initiate the aggregation process, anionic aggregating agents are required. In this study, three salts providing anions, NaCl, Na_2SO_4, and KNO_3 were used as aggregating agents and their effect on SERS activity was investigated.

In case of the Ag nanoparticles, it was found that the adsorption of fonofos onto the Ag surface resulted in a strong SERS signal without requiring any aggregating agent. This indicates that fonofos molecules alone enable the removal of citrate residues adsorbed on the metal surface during the reduction, leading to self-aggregation to the Ag colloids. In practice, a successful formation of the aggregate can be partially predicted by an immediate change in the color of the SERS-active mixture in comparison to the color of its original metal colloidal solution – the turbid gray Ag colloids turned into translucent silvery solutions after addition of fonofos. In comparison, anionic aggregating agents were required to produce fonofos–Au SERS-active aggregates. Among the three anions used in this study, sulfate was found to be the only anion that provided an observable SERS signal of fonofos–Au aggregates. With this combination, the wine-red Au colloids gave rise to a light purple suspension.

Metal nanoparticles exhibit strong absorption features in the UV–visible region as a result of the collective electronic interactions between metal atoms and electrons, the so-called surface plasmons. The characteristics of the plasmon band (i.e. wavelength, bandwidth, and intensity) can therefore be used to provide insights into the particle properties such as size, shape, and concentration. In order to investigate the aggregate formation, UV–visible spectra were measured before and after addition of fonofos into the metal colloidal solutions, and these are shown in Fig. 2. The SERS-active aggregate spectra for both metal nanoparticles show the development of a pronounced shoulder toward longer wavelengths as clearly indicated through the fitted bands (shown in dashed lines). Such a phenomenon confirms the aggregation of particles into clusters of different sizes which are responsible for a range of plasmon frequencies as evidenced by the broadness of the plasmon band in the UV–visible spectra. Using an excitation frequency close to the maxima of the plasmon band can most effectively excite the surface plasmons of the metal–analyte aggregates, thereby producing an optimal SERS response. As a consequence, 633-nm excitation wavelength was employed for the SERS detection of fonofos under such conditions. Moreover, the colloid bands of both metals broaden after adding fonofos and display a slight red-shift of the band maxima (i.e. $\leq$10 nm), consistent with a decrease in inter-particle spacing of the isolated colloids that did not form aggregates with the adsorbate. This implies that the Coulombic repulsion due to the negative surface charge that primarily prevents particles from aggregation is lowered and the forces are dominated by Van der Waals interactions that draw the particles closer.[28] It is also suggested, based on the observed spectral features of the two metal colloids, that Ag colloidal particles produced more and larger aggregates than those of Au.

To investigate the size and morphology of the metal aggregates, transmission electron microscopy (TEM) images of the prepared metal nanoparticles were collected and compared before and after aggregate formation, as shown in Fig. 3. The images display a combination of spherical and rod particles in various shapes and sizes produced in the citrate-reduced Ag colloidal solution, whereas the prepared Au particles are shown to be only spherical

 Copyright © 2010 John Wiley & Sons, Ltd.

and more monodisperse in the suspension. Average diameters of the spherical Ag and Au nanoparticles were found to be 48 and 19.5 nm, respectively, which are both consistent with the sizes of metal spheres required to excite a dipolar plasmon responsible for SERS activity. On the other hand, TEM images of the metal aggregates reveal differences in size and distribution of the aggregates formed by different metal nanoparticles. Similar to the UV–visible results, substantially larger clusters were apparently produced from Ag colloids than those of Au aggregates, which significantly reflect the SERS activity obtained.

SERS spectra

Figure 4 presents SERS spectra of fonofos obtained using Ag and Au colloidal nanoparticles together with its normal Raman spectrum. The SERS spectral profile corresponds very well with the normal Raman spectrum and the enhanced signals clearly indicate the achievement of SERS activity for both metal colloids using 0.01% fonofos (i.e. equivalent to ~10 ppm in the SERS-active mixture), even though the actual concentration of fonofos in the dried film is higher than that of the SERS solution due to concentration upon drying. However, the size of the sampling area should be taken into account and the fact that only dried particles within ~1 μm diameter under a ×50 objective (numerical aperture of 0.75) using a 633-nm excitation wavelength in practice account for the observed Raman scattering signals. No spectral changes that could be associated with sample decomposition were observed. It should be noted that attempts to obtain a normal Raman spectrum of fonofos at the same concentration either through the original methanolic solution or in the form of a dried film failed to produce any fonofos characteristic band. In fact, the SERS spectra of both metal aggregates exhibit three prominent features around 1000–1080 cm^{-1} similar to the result previously published by Lee and Farquharson.[24] The relative intensities of the surrounding bands however differ noticeably when comparing the spectra with the two metal colloids, the normal Raman spectrum and the spectrum of Lee and Farquharson.[24]

In order to more easily demonstrate the changes in relative intensity, spectral normalization was performed on both SERS and normal Raman spectra using the band at 1000 cm^{-1} [i.e. δ(CCC) vibrations of the phenyl ring] as reference. The normalized spectra are shown in Fig. 5 and reveal a close similarity in relative intensities obtained for Au–fonofos aggregates and the normal Raman spectrum albeit with an extrafeature in the SERS spectrum. In contrast, the Ag–fonofos aggregates resulted in a different SERS intensity profile with significant enhancements for the bands at 1582 and 1079 cm^{-1}, but not for the bands in low-wavenumber region (≤850 cm^{-1}) including the prominent single band at 614 cm^{-1} (i.e. γ(CCC) vibration of the phenyl ring). The observed SERS spectral profile of Ag aggregates is however found to be similar to the results published by Lee and Farquharson[24] in which fonofos molecules were adsorbed and detected on the surface of Ag nanoparticles embedded in a sol–gel matrix. There are however wavenumber shifts in some of the major bands and significant differences in the intensities of the weaker bands when compared with the sol–gel matrix SERS. The observed metal-dependent SERS spectral features suggest changes in orientation geometry of the adsorbed fonofos on different metal surfaces, which is possibly due to altered metal–adsorbate interactions.

According to the selection rule of SERS, the normal modes of adsorbed molecules involving changes in molecular polarizability with a component perpendicular to the metal surface are subjected

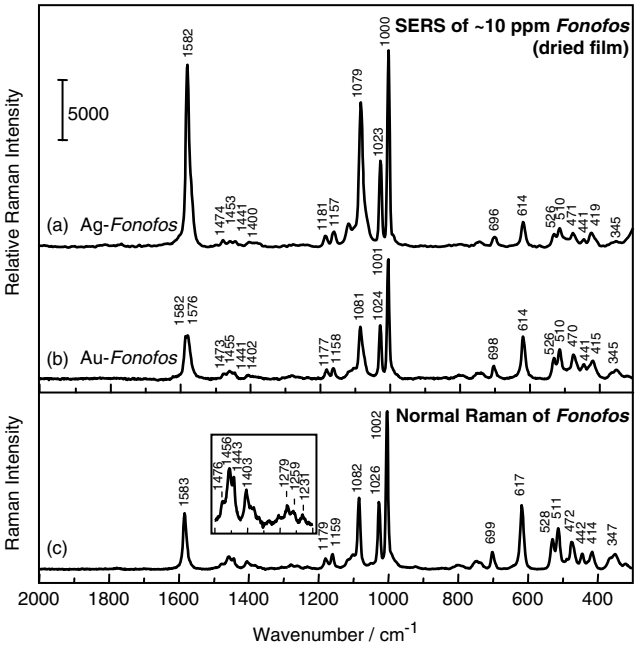

Figure 4. SERS spectra of ~10 ppm fonofos adsorbed on (a) Ag and (b) Au nanoparticles in comparison with (c) normal Raman spectrum measured in a liquid phase using 633-nm excitation wavelength and 10 s exposure time. Note that the SERS spectra are the average of 10 spectra collected at random spots within the dried films under the same experimental conditions.

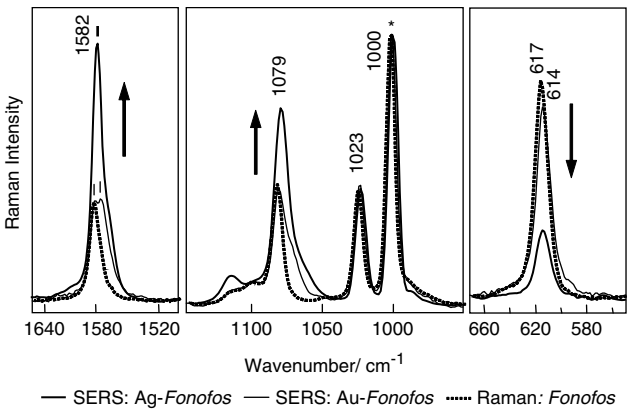

Figure 5. Normalized Raman spectrum of fonofos (dash line) in comparison with normalized SERS spectra of Ag- and Au-aggregates, as represented by thick (—) and thin (–) lines, respectively. Note that the intensity of the band at 1000 cm^{-1}, as marked by (*), was utilized as a reference for spectral normalization.

to the greatest enhancement.[29] The two most strongly enhanced bands present in the Ag–aggregate spectrum are contributed to mainly by ν(C=C) stretching modes of the phenyl ring and the ν(S–C_{phenyl}) stretch in association with δ(C_{phenyl}–H) deformation vibrations, both of which are in the plane of the phenyl ring (see detailed descriptions for modes 66 and 43 in Table 1). The nature of these modes suggests that the phenyl ring is closely associated with the attachment site, but is not parallel with the Ag surface in the manner shown in Fig. 6(b), as is found in benzene[30] or some other aromatic molecules.[31] Rather, it is likely to align in such way that the bond connecting the S atom to the benzene-ring (i.e. S_7–$C_{phenyl\ ring}$) is orientated somewhat perpendicular to

Copyright © 2010 John Wiley & Sons, Ltd.

Journal of RAMAN SPECTROSCOPY

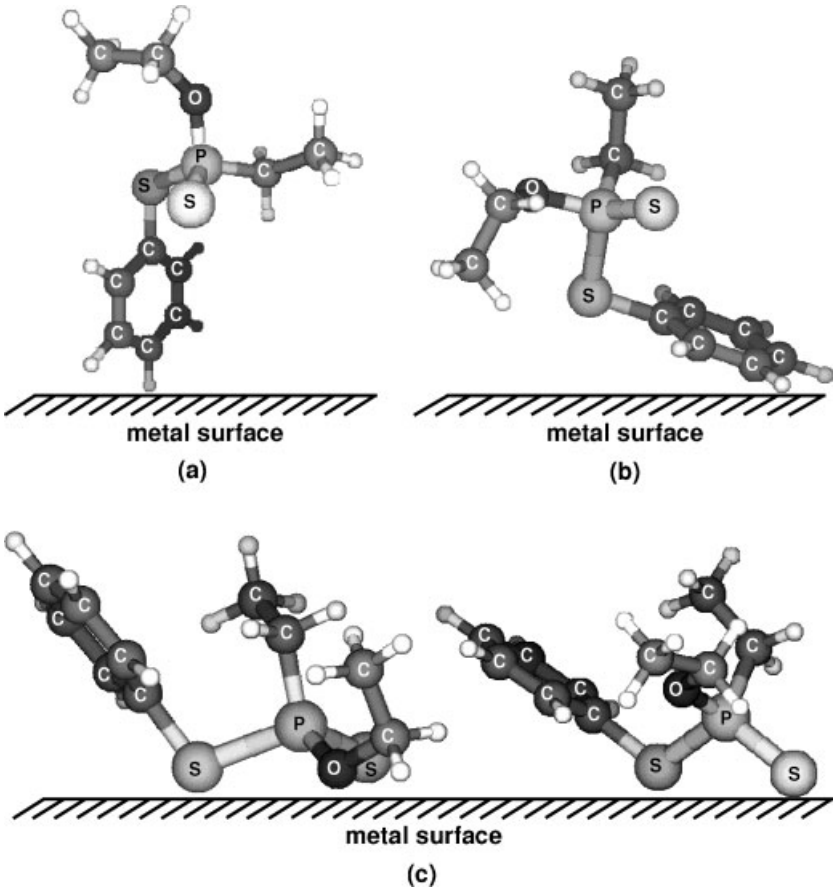

Figure 6. (a and b) Proposed models of the possible molecular orientation of fonofos adsorbed on the metal colloidal surface according to the observed SERS spectral features and the band assignments from the DFT calculations, whereas (c) represents the chemically favorable binding coordinations of fonofos by considering electron affinity between the highly electronegative heteroatoms (S,O) and the metals.

the Ag surface. The structure shown in Fig. 6(a) may satisfy this condition, but it would be fairly unprecedented particularly for the benzene to bind on the metal through C–H sites of the phenyl ring, particularly when electronegative heteroatoms such as sulfur (S) and oxygen (O) are available for binding. Considering their known chemical affinity for Ag, it is probable that at least one of the heteroatoms is linked to the surface. Modifying the most stable structures discussed earlier by rearrangement of the flexible side chains, it is possible to generate structures that could facilitate two or three more such linkages and keep the phenyl ring tilted away from the surface, see for example those in Fig. 6(c). The preliminary DFT calculations on the bare molecule in these structures that yield energies relative to the global minimum of about 50 and 20 kJ mol^{-1} for the triply bound (S,S,O) and the doubly bound (S,S) structures, respectively, are shown in Fig. S2. In both cases, the energy of torsional strain is a modest energetic price to pay in order to optimize a pair of Ag$\cdots$X interactions. For example, the binding energy for a single thiolate bond to an Ag surface has been computed to be over 120 kJ mol^{-1}.[32] Thus, it appears highly likely that the fonofos molecule will rearrange itself on the SERS-active surface to facilitate chemical interactions. A similar trend was inferred in the molecule, 6-mercaptopurine riboside (6-MPR), with semi-empirical calculations suggesting that binding to metals can cause a substantial geometric restructuring giving rise to more energetically favorable coordination.[33]

The normalized SERS spectrum obtained from Au–fonofos aggregates however reveals a pattern of relative intensities remarkably similar to those of the normal Raman spectrum, except for the splitting of the bands at 1576 cm^{-1}. Considering the predicted fundamental vibrational modes acquired from DFT calculations in Fig. 1, the band at 1583 cm^{-1} actually consists of two different ν(C═C) stretching modes of the phenyl ring predicted at wavenumber values close to each other, even though the mode at a higher wavenumber which is used for assigning the band found in the experimentally measured spectra is six times more intense than the other (i.e. modes 66 vs 65 in Table 1). The effect of the surface interaction in Au–fonofos aggregates therefore leads to a significant enhancement of the less dominant ν(C═C) stretching mode at 1575 cm^{-1}. Repeats of a similar experiment were performed with freshly prepared Au colloidal nanoparticles using identical acquisition parameters and under the same experimental conditions, and the result presents a good reproducibility of the splitting features observed only for the Au–fonofos aggregates as shown in Fig. S3 (Supporting Information). To further confirm the splitting of the band, SERS spectra of fonofos were collected using a commercial SERS-active Au substrate[34] (Klarite™, D3 Technologies Ltd, Glasgow, UK), which is composed of a nanostructured patterning of a Au-coated silicon surface with regular arrays of holes. Spectra taken from various spots on the commercial substrate after complete evaporation of methanol showed clearly the enhanced band at 1575 cm^{-1} corresponding to the less dominant mode in the calculated fundamental wavenumber values (data shown in Fig. S4). As a result, this enhanced band appeared to be shifted when

 Copyright © 2010 John Wiley & Sons, Ltd.

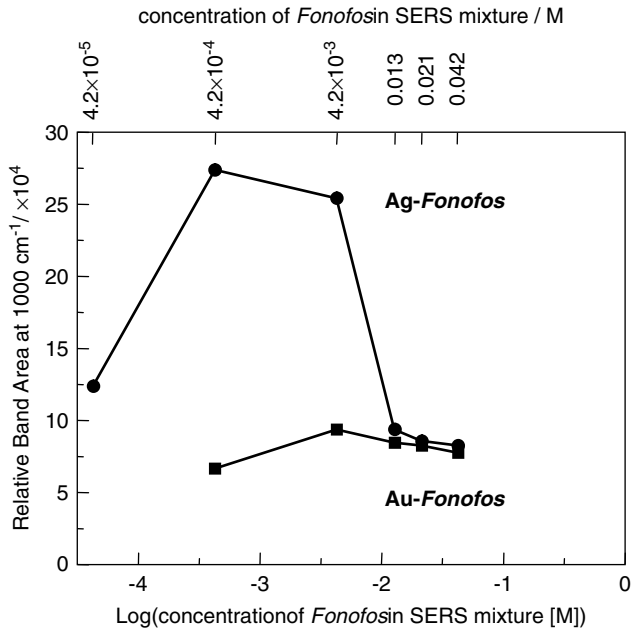

Figure 7. Plot of SERS response of the band at 1000 cm^{-1} obtained from Ag–fonofos (–●–) and Au–fonofos (–■–) aggregates as a function of fonofos concentration in the SERS mixture (log[M]).

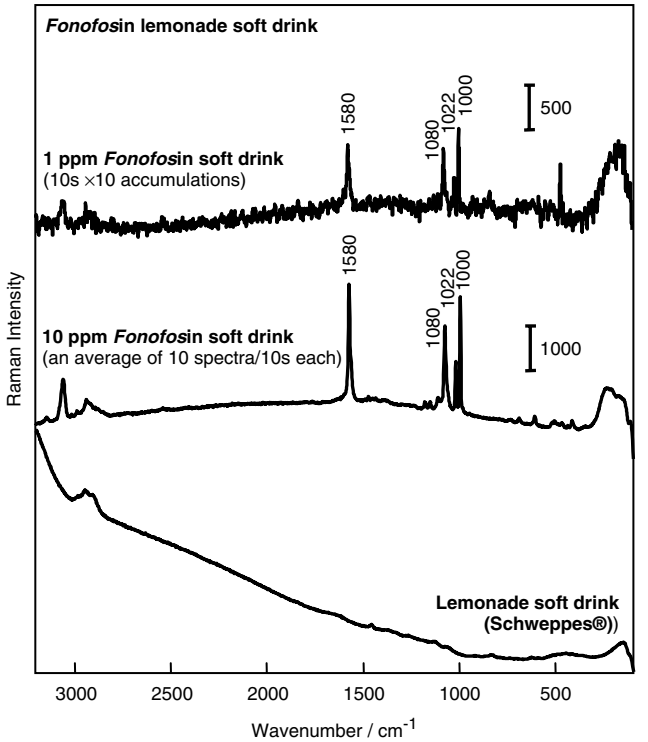

Figure 8. SERS spectra of fonofos detected in a lemonade soft drink (Schweppes®) at concentrations of 1 and 10 ppm shown in comparison to a normal Raman spectrum of the pure lemonade soft drink. All the spectra were measured using 633-nm excitation wavelength. The SERS spectrum of 1-ppm fonofos in lemonade matrix was measured with 10s × 10 accumulations, whereas an average of 10 spectra (10s each) was used for SERS of fonofos-lemonade at 10 ppm. Note that the SERS spectra shown in the figure were subtracted from the corresponding Raman spectrum of the pure lemonade soft drink in order to reduce the background interference from the soft drink.

compared to the normal Raman spectrum in which this mode is suppressed. With just this one spectral change evident from the normal Raman spectrum to that on the Au surface, it is unclear how much of the observed spectrum results from surface plasmon enhancement. The phenyl ring is involved in this change, again indicating its close association with the binding site, but it does appear that the binding arrangement differs somewhat from the Ag colloids.

In addition, a series of concentration-dependent SERS spectra were recorded by varying the original concentration of fonofos in the range of 0.01–10% v/v (i.e. equivalent to 42 μM–42 mM of fonofos in the SERS mixture) to estimate the sensitivity of the technique and to investigate the profile of the SERS response when lowering fonofos concentration. Figure 7 illustrates a plot of the band area measured for the SERS band at 1000 cm^{-1} as a function of fonofos concentration in log [M] unit. The SERS intensities obtained from both metal aggregates are found to be comparable for the three high concentrations (i.e. [fonofos] ≥13 mM). However, SERS signals of the Ag aggregates at concentrations lower than this point produce a drastic increase in enhancement magnitude, which is highest at a fonofos concentration of ~100 ppm (or 0.42 mM), before beginning to fall afterwards. The Au aggregates, on the contrary, produced lower enhancement scale for the entire range of concentrations used in the experiment. However, similar to the Ag aggregates, the SERS profile of Au–fonofos aggregates exhibits an observable increase when the concentration was reduced to ~1000 ppm equivalent to 4.2 mM (i.e. log [M] = −2.4) prior to the presence of a sharp incline when the concentration was further decreased beyond this point. Therefore, the sensitivity of the technique has been demonstrated herein to be capable of detecting fonofos in parts per million range using metal colloids with a superior sensitivity achieved by the use of Ag nanoparticles. Even though the observed nonlinear relationship between SERS response and concentration of the analyte indicates a difficulty in applying the technique for quantitative analysis, such information is, nevertheless, essential in understanding the metal–adsorbate interactions involving in the SERS enhancement mechanism as this will elucidate the physical basis of signal enhancement prior to developments of SERS-active substrates with a rational design that is applicable for quantitative measurements.

Concerning the SERS efficiency achieved by the two metals, based on the band at 1000 cm^{-1} the SERS intensity of Au–fonofos aggregates, as shown in Fig. 4(b), is apparently about half of that produced by Ag nanoparticles under the same SERS conditions, indicating a stronger interaction produced between Ag–fonofos aggregates. By taking the results from UV–visible spectroscopy and TEM into account, the lower SERS signals are possibly attributed to reduced interaction between fonofos and Au to form active aggregates, causing the resultant aggregates to be small in size and quantity. In contrast, the Ag–fonofos aggregates were found in considerably large clusters and a significantly higher SERS enhancement was obtained. However, it should be emphasized that attempts to add aggregating agents (i.e. sulfate, nitrate, and chloride anions) to improve the aggregation process did not yield a substantial SERS intensity – no signal of fonofos was detected in case of chloride anion, but SERS signatures were observed for sulfate and nitrate anions at lower enhancements. Therefore, the optimal condition to achieve highest SERS response for fonofos is found to be with the use of Ag colloidal nanoparticles without the aid of any aggregating agent.

Copyright © 2010 John Wiley & Sons, Ltd.

From the theoretical point of view, our findings are in good agreement with previous theoretical and semi-empirical studies based on EM field enhancements in two-dimensional arrays of metal nanoparticles embedded in a dielectric medium where the maximum EM enhancement factor produced by Ag was found to be four times larger than that of Au.[35,36] The reported numerical EM calculations utilizing the Drude free-electron model clearly demonstrated that differences in SERS response between the two metals are intrinsically influenced by the optical properties of materials (i.e. dielectric functions of metal and the medium) in addition to the extrinsic factor of chemical effects from the target adsorbates. The theoretical investigations also revealed a critical relationship between particle size and inter-particle spacing on the calculated EM enhancement. By taking this into consideration, the observed denser clusters of the SERS-active Ag–fonofos aggregates, which in turn suggest a closer interparticle spacing as compared to those formed by Au colloids, conform to the theory and therefore a higher enhancement is expected for Ag than Au.

SERS detection of fonofos in a lemonade soft drink using Ag colloidal nanoparticles

In order to test the application of SERS in trace analysis, a trial experiment was performed to detect fonofos in a carbonated lemonade soft drink (Schweppes®) starting at ~10 ppm concentration using the prepared Ag colloidal solution. In practice, the container of the soft drink was left open overnight before the experiment or until the carbon dioxide dissipated as evidenced by an absence of bubbles and a clear flat top surface. The drink, which possessed an original pH of 3.5, was brought to a neutral pH using 0.1 M NaOH prior to adding fonofos and mixing into an aliquot of Ag colloidal solution. Figure 8 demonstrates the SERS spectra collected from a dried film of the soft drink being treated as mentioned above, in comparison to the Raman spectrum of an untreated soft drink. Interestingly, the SERS spectra present clearly the fonofos signature without any noticeable interference from other additives contained in the drink (such as sugar, caffeine, flavorings, colors, preservatives), even though the signal achieved appears to be substantially lower than that observed in SERS of pure fonofos at the same concentration and under the same acquisition parameters (see Fig. 4(a) for comparison). Nevertheless, the observation indicates that fonofos itself has a sufficient affinity to replace the citrate residue and to overcome other components in the same matrix to achieve a strong binding onto the Ag colloidal surfaces. It should however be noted that the intensity of the signals varied substantially from one aggregate to another. In addition to spectral averaging method, a long accumulation was essentially required to achieve an observable signal and thereby a sufficient spectral quality particularly at a very low concentration (e.g. the use of 10 s × 10 accumulations for detecting 1-ppm fonofos in lemonade). Our trivial experiment ultimately indicates a good sensitivity and a high selectivity of the SERS technique in detecting fonofos even at the concentration as low as just ~1 ppm. The result demonstrates a potential for the technique to be a promising alternative in trace analysis such as a detection of pesticide residue in fruit-based drinks.

Conclusion

We have demonstrated here the applications of the SERS technique in trace analysis of hazardous OPPs at ppm levels using fonofos as a model analyte. The observed SERS spectral profiles indicate that the orientation geometry of the adsorbed fonofos molecules depends on the type of metal colloids. Detailed studies based on DFT calculations reveal an insight into active binding sites and geometry of the adsorbed fonofos on the surface of certain metals. The findings provide an understanding of the metal-induced binding structure of the adsorbed fonofos for further developments of SERS-active substrates, as well as for practical applications of the technique in residue analysis of food contaminants.

Acknowledgements

This work is financially supported by the Rural Industry Research and Development Corporation (RIRDC). The DFT calculations were performed through the computers at the Australian Partnership for Advanced Computing (APAC) National Facility. We also gratefully acknowledge Mr Finlay Shanks for assistance with the instrumentations and Dr Peter Godfrey for carrying out the initial computational predictions.

Supporting information

Supporting information may be found in the online version of this article.

References

[1] M. A. Kamrin, in *Pesticide Profiles: Toxicity, Environmental Impact, and Fate*, (Ed.: M. A. Kamrin), CRC Press: Boca Raton, **1997**.
[2] V. K. Jha, D. S. Wydoski, in *U.S. Geological Survey Water-Resources Investigations Report 02-4222*, U.S. Geological Survey, Denver, CO, **2003**.
[3] L. V. Podhorniak, J. F. Negron, F. D. Griffith, Jr, *J. AOAC Int.* **2001**, *84*, 873.
[4] A. Colume, S. Cardenas, M. Gallego, M. Valcarcel, *J. Chromatogr. A* **1999**, *849*, 235.
[5] E. Ueno, H. Oshima, I. Saito, H. Matsumoto, *J. AOAC Int.* **2003**, *86*, 1241.
[6] E. Ueno, H. Oshima, I. Saito, H. Matsumoto, Y. Yoshimura, H. Nakazawa, *J. AOAC Int.* **2004**, *87*, 1003.
[7] J. L. Martinez-Vidal, F. J. Arrebola, M. Mateu-Sa'nchez, *J. Chromatogr. A* **2002**, *959*, 203.
[8] D. Ortelli, P. Edder, C. Corvi, *Anal. Chim. Acta* **2004**, *520*, 33.
[9] C. Jansson, T. Pihlström, B. G. Österdahl, K. E. Markides, *J. Chromatogr. A* **2004**, *1023*, 93.
[10] M. Fleischmann, P. J. Hendra, A. J. Mcquilla, *J. Chem. Phys. Lett.* **1974**, *26*, 163.
[11] J. M. Chalmers, P. R. Griffiths, *Handbook of Vibrational Spectroscopy*, John Wiley & Sons: New Jersey, **2002**.
[12] S. Nie, S. R. Emory, *Science* **1997**, *275*, 1102.
[13] K. Kneipp, Y. Wang, H. Kneipp, L. T. Perelman, I. Itzkan, R. R. Dasari, M. S. Feld, *Phys. Rev. Lett.* **1997**, *78*, 1667.
[14] M. Moskovits, *Rev. Mod. Phys.* **1985**, *57*, 783.
[15] FDA, *Food and Drug Administration Pesticide Program Residue Monitoring*, United States Food and Drug Administration: Washington, **1996**.
[16] P. C. Lee, D. Meisel, *J. Phys. Chem.* **1982**, *66*, 3391.
[17] R. A. Alvarez-Puebla, E. Arceo, P. J. G. Goulet, J. J. Garrido, R. F. Aroca, *J. Phys. Chem. B* **2005**, *109*, 3787.
[18] C. H. Munro, W. E. Smith, M. Garner, J. Clarkson, P. C. White, *Langmuir* **1995**, *11*, 3712.
[19] M. K. Chow, C. F. Zukoski, *J. Colloid Interface Sci.* **1994**, *165*, 97.
[20] *GRAMS/32, Version 4.14*, G. I. Corporation: Salem, **1991**.
[21] M. J. Frisch, G. W. Trucks, H. B. Schlegel, G. E. Scuseria, M. A. Robb, J. R. Cheeseman, J. A. Montgomery, Jr, T. Vreven, K. N. Kudin, J. C. Burant, J. M. Millam, S. S. Iyengar, J. Tomasi, V. Barone, B. Mennucci, M. Cossi, G. Scalmani, N. Rega, G. A. Petersson, H. Nakatsuji, M. Hada, M. Ehara, K. Toyota, R. Fukuda, J. Hasegawa,

Copyright © 2010 John Wiley & Sons, Ltd.

M. Ishida, T. Nakajima, Y. Honda, O. Kitao, H. Nakai, M. Klene, X. Li, J. E. Knox, H. P. Hratchian, J. B. Cross, V. Bakken, C. Adamo, J. Jaramillo, R. Gomperts, R. E. Stratmann, O. Yazyev, A. J. Austin, R. Cammi, C. Pomelli, J. W. Ochterski, P. Y. Ayala, K. Morokuma, G. A. Voth, P. Salvador, J. J. Dannenberg, V. G. Zakrzewski, S. Dapprich, A. D. Daniels, M. C. Strain, O. Farkas, D. K. Malick, A. D. Rabuck, K. Raghavachari, J. B. Foresman, J. V. Ortiz, Q. Cui, A. G. Baboul, S. Clifford, J. Cioslowski, B. B. Stefanov, G. Liu, A. Liashenko, P. Piskorz, I. Komaromi, R. L. Martin, D. J. Fox, T. Keith, M. A. Al-Laham, C. Y. Peng, A. Nanayakkara, M. Challacombe, P. M. W. Gill, B. Johnson, W. Chen, M. W. Wong, C. Gonzalez, J. A. Pople, *Gaussian 03, Revision D.01*, Gaussian, Inc.: Wallingford, CT, **2004**.

[22] V. Krishnakumar, G. Keresztury, T. Sundius, R. Ramasamy, *J. Mol. Struct.* **2004**, *702*, 9.

[23] D. Michalska, R. Wysokiński, *Chem. Phys. Lett.* **2005**, *403*, 211.

[24] Y. H. Lee, S. Farquharson, *Proc. SPIE Int. Soc. Opt. Eng.* **2001**, *4206*, 140.

[25] C. Shende, A. Gift, F. Inscore, P. Maksymiuk, S. Farquharson, *Proc. SPIE Int. Soc. Opt. Eng.* **2004**, *5271*, 28.

[26] S. Li, D. Wu, X. Xu, R. Gu, *J. Raman Spectrosc.* **2007**, *38*, 1436.

[27] M. Alcolea Palafox, *Int. J. Quantum Chem.* **2000**, *77*, 661.

[28] M. Meyer, E. C. Ru, P. G. Etchegoin, *J. Phys. Chem. B* **2006**, *110*, 6040.

[29] J. A. Creighton, in *Spectroscopy of Surfaces* (Eds: R. J. H. Clark, R. E. Hester), John Wiley & Sons: Chichester, **1988**.

[30] X. Gao, J. P. Davies, M. J. Weaver, *J. Phys. Chem.* **1990**, *94*, 6858.

[31] M. Fleischmann, I. R. Hill, G. Mengoli, M. M. Musiani, *Electrochim. Acta* **1983**, *28*, 1545.

[32] J. Meyer, T. Bredow, C. Tegenkamp, H. Pfnüra, *J. Chem. Phys.* **2006**, *125*, 194705.

[33] O. Martínez, A. Vivoni, Z. Qiao, U. Udeochu, C. M. Hosten, *Surf. Sci.* **2006**, *600*, 1787.

[34] N. M. B. Perney, J. J. Baumberg, M. E. Zoorob, M. D. B. Charlton, S. Mahnkopf, C. M. Netti, *Opt. Express* **2006**, *14*, 847.

[35] D. A. Genov, A. K. Sarychev, V. M. Shalaev, A. Wei, *Nano Lett.* **2004**, *4*, 153.

[36] H. C. Kim, X. Cheng, *Opt. Express* **2009**, *17*, 17234.

Copyright © 2010 John Wiley & Sons, Ltd.